ELSEVIER

International Journal of Mass Spectrometry 223–224 (2003) 141–158

International Journal of Mass Spectrometry

www.elsevier.com/locate/ijms

The influence of electron impact ionisations on low frequency instabilities in a magnetised plasma

Dan-Gheorghe Dimitriu[a,b], Valerian Ignatescu[a,b], Codrina Ioniţă[a], Erzilia Lozneanu[a,b], Mircea Sanduloviciu[a,b], Roman W. Schrittwieser[a,*]

[a] *Department of Ion Physics, University of Innsbruck, Technikerstr. 25, A-6020 Innsbruck, Austria*
[b] *Faculty of Physics, University "A.I. I. Cuza," RO-6600 Iasi, Romania*

Received 8 January 2002; accepted 18 March 2002

To the memory of the late Werner Lindinger, a wonderful colleague and friend.

Abstract

We report new results on the interaction of the potential relaxation instability with the electrostatic ion–cyclotron instability in a magnetised alkaline plasma. The simultaneous excitation of these instabilities, accompanied by an amplitude and frequency modulation of the latter by the former, gives rise to the appearance of sidebands in the spectrum, which are situated on both sides of the ion–cyclotron instability frequency with a frequency difference equal to the potential relaxation instability frequency. In addition, our experimental data prove that the ion–cyclotron instability frequency not only shows the familiar increase with the magnetic field strength but also decreases with the collector current. It turns out that the spacing of the sidebands on the frequency axis is in keeping with the current oscillations. This is explained by the possibility of additional electron-neutral impact ionisations by fast electrons in front of the positively biased end electrode. The non-linear dynamical analysis of the signals gives some information about the state space dynamics of our system. (Int J Mass Spectrom 223–224 (2003) 141–158)

Keywords: Plasma instabilities; Non-linear interaction; Sidebands; Excitation; Ionisation

1. Introduction

"Quiescent plasma machines" (Q-machines) were developed as laboratory plasma sources in order to produce a quiescent plasma [1,2], i.e., a plasma that is inherently free from low frequency instabilities, unless they are excited on purpose. These devices were extensively used for fundamental investigations of transport phenomena and diffusion of particles along and across the magnetic field lines [3], linear and non-linear wave propagation [4,5], plasma stability [6], the general behaviour of a bounded plasma system [7] and the formation of non-linear potential structures such as space charge double layer [8–10]. Under well defined external experimental conditions, the plasma of a Q-machine becomes unstable and a variety of mainly electrostatic instabilities can be excited. Among those are the drift instability [11], the Kelvin–Helmholtz instability [12], the electrostatic ion–cyclotron instability (EICI) [13–15], the inhomogeneous energy–density driven instability [16] and the potential relaxation instability (PRI) [8,17–20].

* Corresponding author. E-mails: dimitriu@uaic.ro, igvaly@yahoo.com, codrina.ionita@uibk.ac.at, erloz@uaic.ro, msandu@uaic.ro, roman.schrittwieser@uibk.ac.at

1387-3806/02/$ – see front matter
PII S1387-3806(02)00786-8

These instabilities appear as coherent oscillations of the plasma parameters, sometimes showing a strongly non-linear behaviour [21–25].

The PRI and the EICI are excited by drawing an electron current parallel to the magnetic field to a circular collector, which is inserted into the plasma column perpendicular to the axis. For exciting the PRI, the radius of the collector has to be sufficiently larger than the ion gyroradius so that the ion trajectories can be considered as one-dimensional. For exciting the EICI, the radius of the collector must be considerably smaller than that of the plasma column, but still in the range of a few ion gyroradii. A transition from the PRI into the EICI by decreasing the diameter of the collector was reported earlier [26]. A certain range of collector radii, where both instabilities could be excited simultaneously, was found. This phenomenon led to an amplitude modulation of the EICI by the PRI, with the amplitude of the latter being much larger than that of the former. Both instabilities lead to strong modulations of the electron current through the plasma, however, on different frequency scales. The PRI frequency is mainly controlled by the ion transit time through the entire system, whereas the EICI frequency is slightly higher than the ion gyrofrequency. Thus, in a Q-machine f_{EICI} is usually about one order of magnitude larger than f_{PRI}.

We report on an investigation in the magnetised alkaline plasma of a single-ended Q-machine where both instabilities, PRI and EICI, are excited simultaneously with comparable amplitudes by gradually increasing the bias of the collector, with the EICI appearing at first, and later the PRI. This led to a strong modulation of the EICI by PRI, which affected not only the amplitude but also the frequency of the EICI. Because of this, in the spectrum appear sidebands around f_{EICI} with a frequency difference equal to $\pm f_{\mathrm{PRI}}$.

In addition, we have found a linear decrease of the EICI frequency with increasing collector current. The analysis of the modulated signals has allowed us to make an estimation of the periodical EICI frequency shift, which is concomitant with the formation of the sidebands. The obtained results are in good agreement with the measured amplitude and frequency modulation of the collector current. The current–voltage characteristic of the exciting collector shows abrupt jumps when the EICI and the PRI, respectively, appear, accompanied by hysteresis. This is an indication that the well known oscillating non-linear potential structures, which appear in the plasma column when an electron current is drawn through it, involve electron impact excitation and ionisation reactions. These occur in front of the collector where accelerated electrons suffer inelastic collisions with the alkaline vapour present in the plasma column [22]. A comprehensive non-linear dynamical analysis of the recorded signals gives us a broad picture of the state space dynamics of our system.

2. Experimental set-up

The experiments were performed in the Innsbruck single-ended Q-machine in a potassium plasma, produced by the combined effect of thermionic electron emission from and contact ionisation on a 6 cm diameter tungsten hot plate, heated to about 2200 K (see Fig. 1 for a schematic of the set-up). For this purpose a neutral K-beam was directed to the front side of the hot plate by means of an array of nozzles around the hot plate about 2 cm in front of it. The background pressure of the residual gases (mainly O_2, N_2 and H_2O and carbon hydrates) was less than 10^{-5} mbar. The plasma density was in the range $10^8\,\mathrm{cm}^{-3} < n_{\mathrm{pl}} < 10^9\,\mathrm{cm}^{-3}$, and the ion and electron temperatures were $T_{\mathrm{i}} \cong T_{\mathrm{e}} \cong 0.2$ eV. The confining magnetic field was $0.05\,\mathrm{T} < B < 0.2\,\mathrm{T}$. A circular tantalum limiter, inserted 3.6 cm in front of the hot plate, reduced the diameter of the plasma column to 3.5 cm, thus providing a flatter and more symmetric radial density profile.

At a distance of $d = 27.5$ cm from the hot plate a heatable tantalum collector of 1 cm diameter was inserted into the plasma column. The heating was necessary to prevent coating by potassium, which would alter the work function of the collector, thereby changing the contact potential and shifting the current–voltage characteristic [27]. By biasing this collector positively, an electron current was drawn

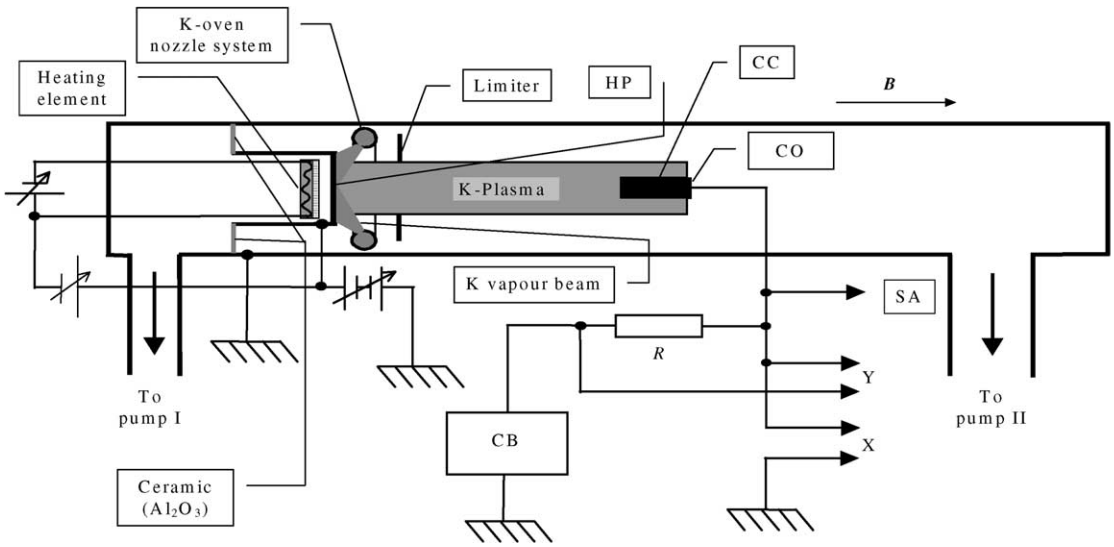

Fig. 1. Schematic of the Innsbruck single-ended Q-machine. HP—hot plate (plasma source), CO—collector, CC—current channel, CB—collector bias (by means of a signal generator or the like), SA—spectral analyser, X/Y—to XY recorder.

through a channel of roughly the same diameter as the collector. Outside this current channel, the plasma was not terminated, except eventually by the walls of the vacuum chamber in a distance of about 90 cm from the hot plate, outside the homogeneous magnetic field region, i.e., in a strongly diverging magnetic field. Similar experiments have also been done with a ring surrounding the collector of an inner diameter of 10.5 mm and an outer one of 70 mm [24]. As long as this ring was left floating, there was no difference in the behaviour of the plasma between this case and the aforementioned one.

3. Experimental results

Fig. 2 shows a typical current–voltage characteristic $I_{co}(V_{co})$ of the collector for the case where in a certain range the two aforementioned instabilities, the EICI [13] and the PRI [20], have been excited simultaneously. Due to the strong magnetic field, the current I_{co} originates from the current channel in front of the collector, extending toward the hot plate. The numbers indicate the values of the collector bias V_{co} where time series of the AC component of I_{co} and FFTs of them have been recorded, either during the increase or during the subsequent decrease of V_{co} (see Figs. 3 and 4, respectively, where the numbers of the signals and FFTs correspond to the numbers on the current–voltage characteristic in Fig. 2). The characteristic shows a downward and an upward jump of the current, when first the EICI and then the PRI appear. The thresholds of the instabilities are marked on the Fig. 2 with large arrows. Because of random phenomena the threshold of both instabilities are not always precisely the same for each time when the respective thresholds are surpassed. The current jumps are obviously due to abrupt changes of the conductivity of the plasma column. The characteristic shows a strong hysteresis around $V_{co} \cong 0\,V$ when V_{co} is gradually increased and then decreased. More details about this hysteresis and the associated current jumps can be found elsewhere [23,24].

The FFTs of the signals show that the first instability, which appears with a considerable amplitude for $V_{co} \cong -1.5\,V$, is the EICI (cf. Fig. 4, FFT #2) with a frequency above the ion gyrofrequency, i.e., $f_{EICI} \cong 67\,kHz$. For potassium and $B \cong 0.13\,T$ the

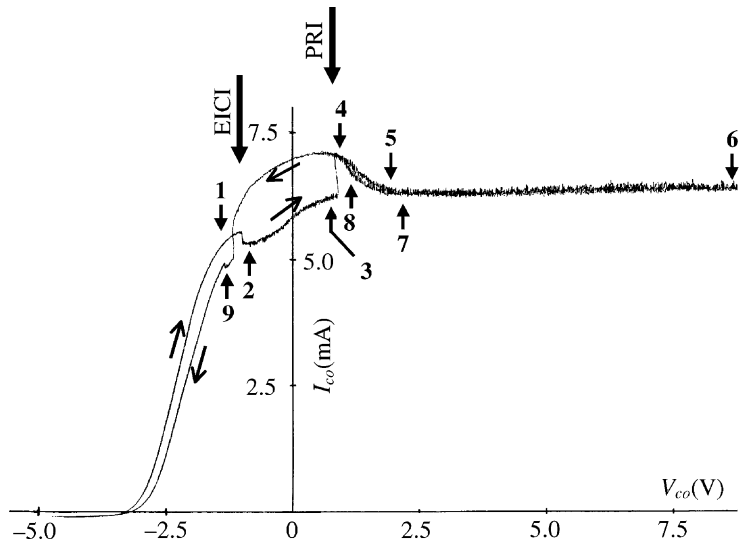

Fig. 2. Typical upward and downward current–voltage characteristic of the collector for $n \cong 10^9\,\mathrm{cm}^{-3}$, $B = 0.13\,\mathrm{T}$, $d = 27.5\,\mathrm{cm}$, $p \cong 3.3 \times 10^{-6}\,\mathrm{mbar}$. The numbers with arrows indicate the positions where the time series and the FFTs have been taken (see Figs. 3 and 4). The large arrows show the onset of the EICI and of the PRI, respectively.

ion gyrofrequency is $\Omega_\mathrm{i}/2\pi \cong 51\,\mathrm{kHz}$ and the ion gyroradius is $r_\mathrm{i} \cong 2.2\,\mathrm{mm}$. Thus $f_\mathrm{EICI} \cong 1.3\Omega_\mathrm{i}/2\pi$, and the collector radius, normalised to the ion gyroradius, is $R \equiv r_\mathrm{co}/r_\mathrm{i} \cong 2.3$ [26]. This frequency is higher than previous results, where seldom more than

$$f_\mathrm{EICI} \cong 1.2\frac{\Omega}{2\pi} = 0.19\frac{eB}{m_\mathrm{i}}, \tag{1}$$

(with m_i being the ion mass) was found [13]. Nevertheless, the identity of the EICI has been thoroughly proved by measuring the well known linear increase of the frequency with the magnetic field strength B according to Eq. (1). Moreover, the EICI has a very low threshold [13,28], and according to [26], the above value of R is very favourable for a strong excitation of the EICI.

Before attaining $V_\mathrm{co} \cong +1\,\mathrm{V}$ (Fig. 4, FFT #4), traces of the PRI appear with a frequency of about 15 kHz. Also this frequency for the given length of the system of $d = 27.5\,\mathrm{cm}$ is higher than earlier results, which yielded

$$f_\mathrm{PRI} \cong a\frac{v_\mathrm{a}}{d} = \frac{a}{d}\sqrt{\frac{k_\mathrm{B}T_\mathrm{e}}{m_\mathrm{i}}}, \tag{2}$$

(with v_a being the ion-acoustic speed and k_B the Boltzmann constant). a is a constant factor in the range of 2–4, related to the speed of ambipolar diffusion and to the duration of the high potential state during one period of the PRI [19,29]. But yet we are convinced to have identified the PRI. Especially under the given conditions, as being excited in a relatively small current channel, and at low plasma densities, the PRI can also appear with higher frequencies [26,30,31].

For increasing V_co, the PRI amplitude grows, and from now on the system has two possible resonances, one at the PRI, one at the EICI frequency, which can be coupled or can be independent from each other. When the PRI amplitude attains the same order of magnitude as that one of the EICI, the interaction between the two instabilities leads to a strong modulation of the latter by the former, not only in amplitude but also in frequency, and consequently also sidebands around f_EICI are formed with a frequency $f_\mathrm{EICI} \pm f_\mathrm{PRI}$. These can be seen in the FFTs #5–#8 of Fig. 4. The amplitude and frequency modulation can be observed in Fig. 5(a), which shows the time series taken in point 7 (corresponding to FFT #7 of Fig. 4, showing

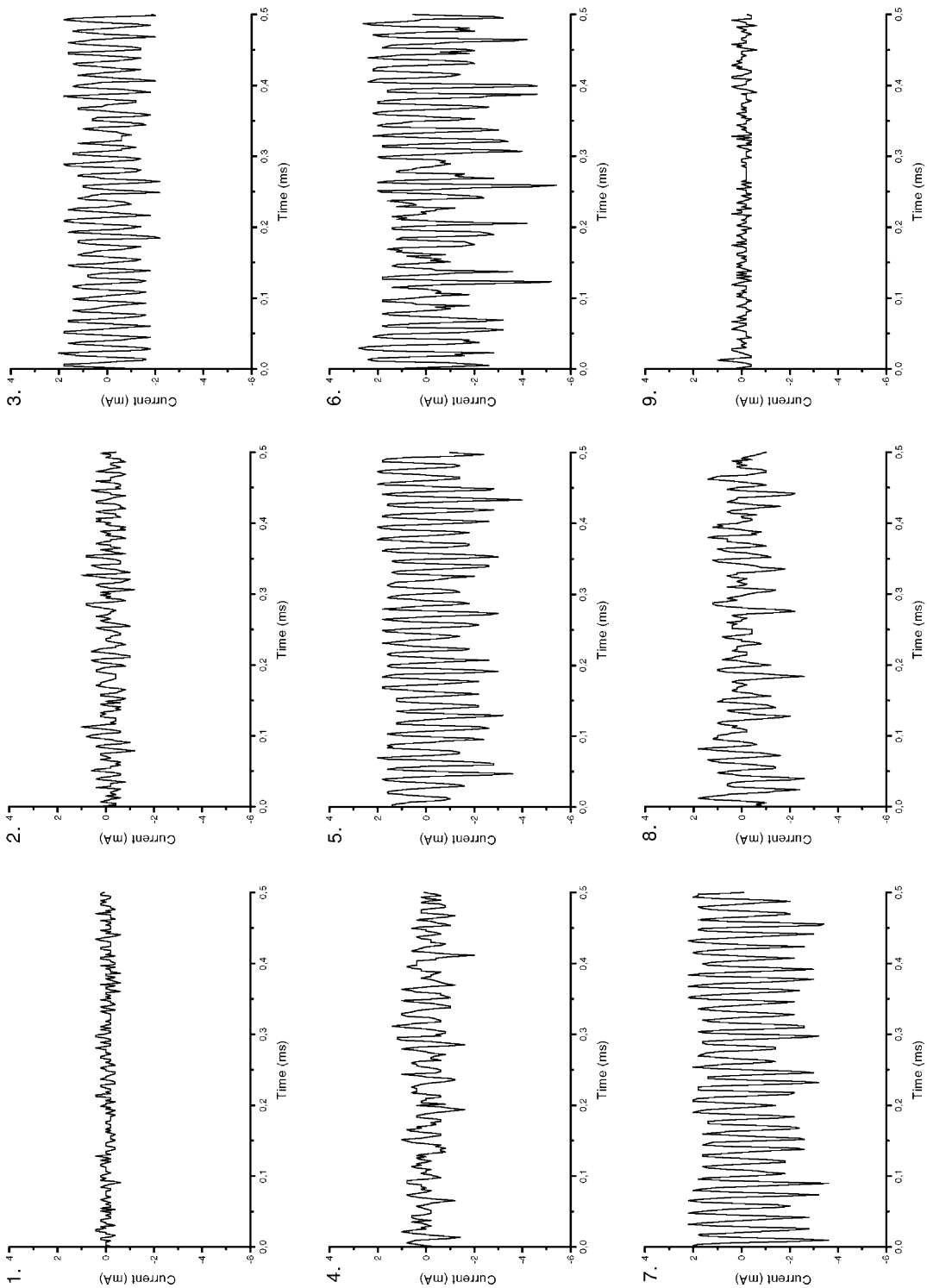

Fig. 3. Time series of the AC component taken at the V_{co} values indicated by the respective numbers in Fig. 2.

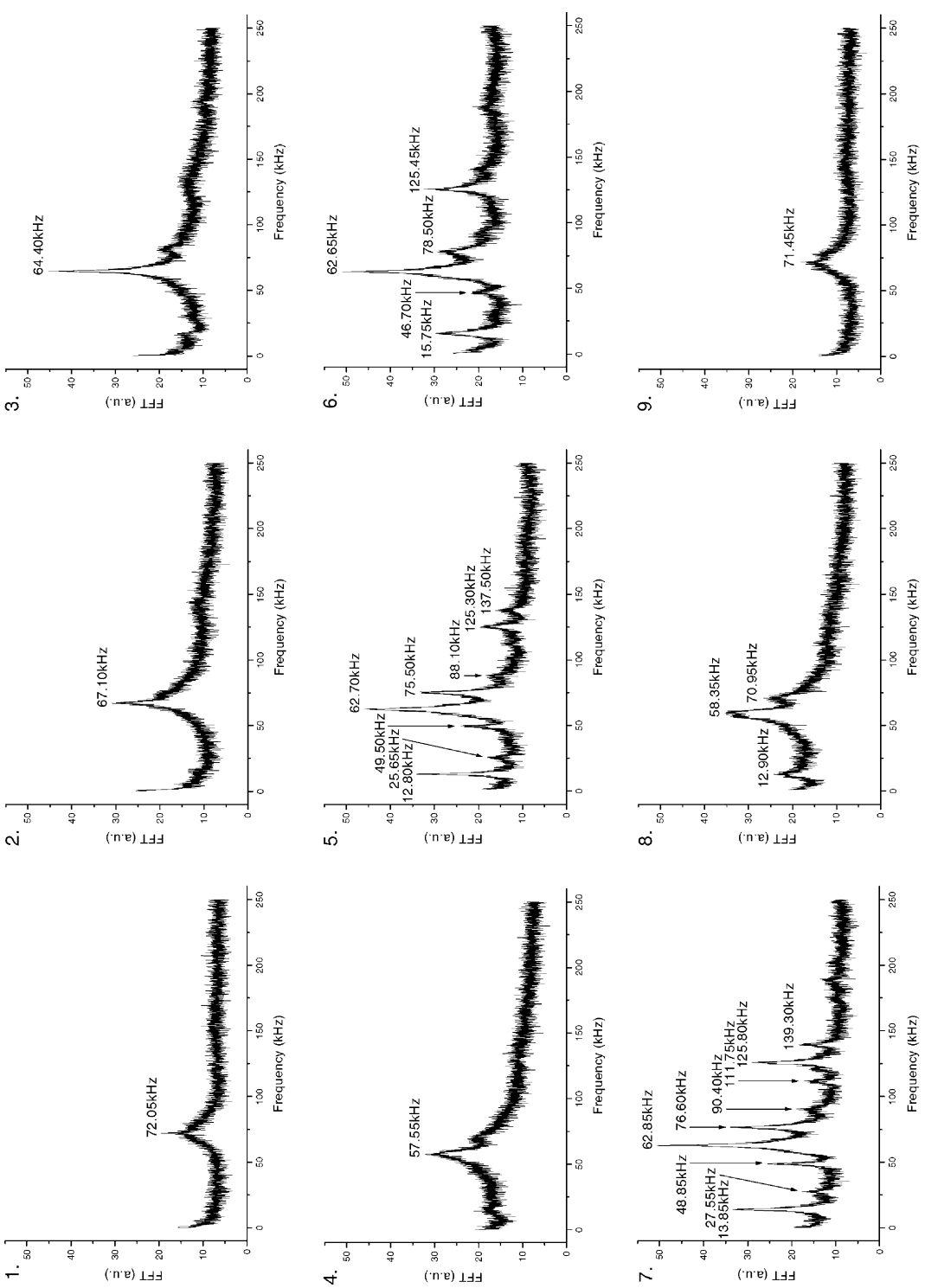

Fig. 4. FFTs of the AC component taken at the V_{CO} values indicated by the respective numbers in Fig. 2.

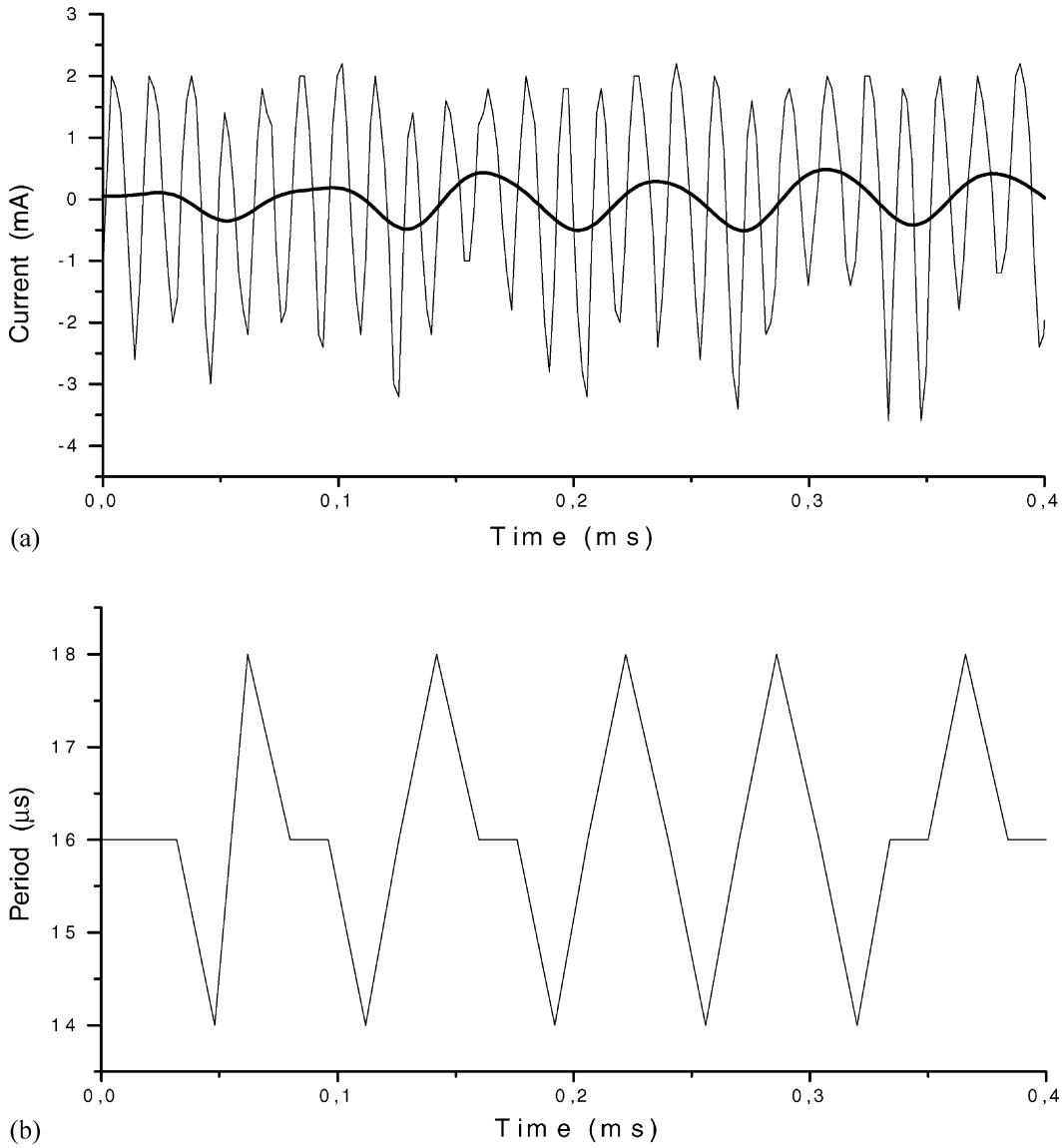

Fig. 5. (a) Time series of the collector current taken at point 7 of the characteristic of Fig. 2. The solid line shows the time average over the high frequency oscillation (EICI). (b) Temporal behaviour of the period of the high frequency oscillation (EICI).

$f_{EICI} \cong 62.5$ kHz) of the characteristic (Fig. 2) for decreasing collector voltage V_{co}. The thick solid line shows the collector current I_{co} after averaging over the EICI frequency. From a comparison of the currents of Fig. 5(a) and of Fig. 2 (which are both on absolute scales in milliamperes) we infer that the relative amplitude of the oscillations is in the range of 0.3 to 0.6. Such high amplitudes are in keeping with previous results [13]. The amplitude modulation of the time series with the PRI frequency is obvious in the time series of Fig. 5(a), where it affects, however, more strongly the negative excursions of the current. The upward excursions of the oscillating current are always much less pronounced, a fact which appears in all the time

series, sometimes even as an absolute limitation of the collector current, especially for higher values of V_{co} so that the positive amplitude seemed to be clipped off. A current limitation due to the formation of thermal barriers in front of a periodically travelling double layer, is a well known feature of both instabilities [8,13,15].

In order to make the frequency modulation better visible, Fig. 5(b) shows the period of the EICI oscillation on the same time scale as the actual time series. We observe that the period in the amplitude maxima is shorter than in the minima by a value of about 4 ms. Thus there is also a frequency modulation of the EICI so that the f_{EICI} becomes higher than the average value of 62.5 kHz in the amplitude maxima (attaining $f_{EICI} \cong 71.4$ kHz) and lower in the minima (attaining $f_{EICI} \cong 55.6$ kHz). By averaging over the EICI period (cf. the thick line in Fig. 5(a)) we see that I_{co} also oscillates with the PRI frequency in such a way that during the maxima of the EICI amplitude (i.e., where also the EICI frequency attains maxima) the collector current is smaller by about 1 mA than in the amplitude and frequency minima.

From the FFTs of Fig. 4 and from the current–voltage characteristic in Fig. 2, the dependence of the EICI frequency on the time average collector current I_{co} has been determined. Fig. 6 shows this relation, and we see that the EICI frequency drops with increasing current and is roughly negatively proportional to it. The solid straight line is a linear fit of the experimental data according to the formula

$$f_{EICI} = -5.76 I_{CO} + 98.82. \quad (3)$$

A decrease of the amplitude and of the frequency with increasing collector current was also found earlier [13,32].

The formation of sidebands in the FFTs is concomitant with the observed frequency modulation of the EICI by the PRI. The upper and lower frequencies in Fig. 5 correspond roughly to the sidebands in the FFT #7 of Fig. 4. We assume that the frequency shift in both directions is due to the modulation of the collector current by the PRI. The modulation of the EICI frequency in Fig. 5(a) with about 15.8 kHz corresponds to a current oscillation between about 7.5 and 4.8 mA. From the thick solid line in Fig. 5(a) we see that there I_{co} oscillates with an amplitude of about 1 mA up and down. Although the frequency modulation is smaller, the general trend is obvious.

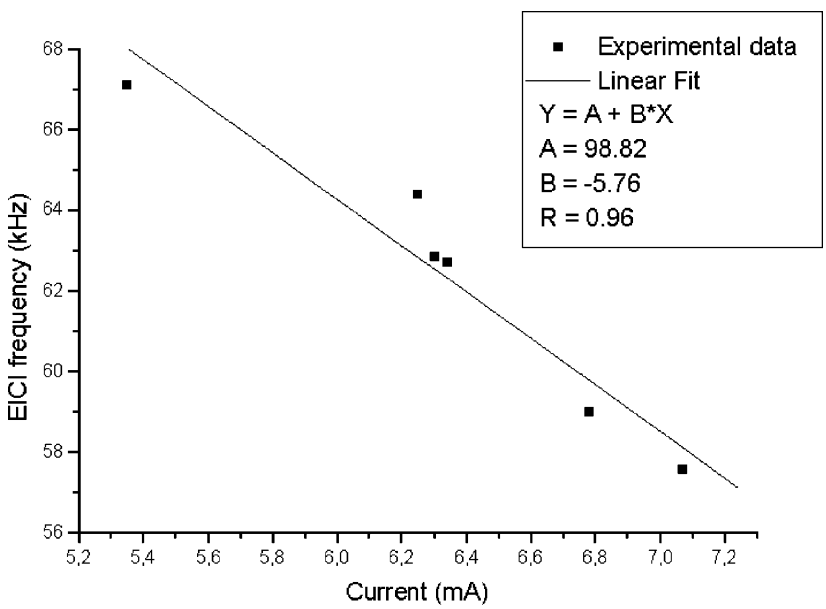

Fig. 6. Dependence of the EICI frequency on the collector current. R is the correlation coefficient of the linear regression.

4. Non-linear dynamical analysis

The non-linear dynamical analysis provides us with powerful tools for analysing the evolution of a non-linear system such as time histories, histograms, Fourier spectra, state space plots, Poincaré maps, autocorrelation functions, Lyapunov exponents, dimension calculations, etc. Since the phenomena studied here are clearly strongly non-linear, we presume that a non-linear dynamical analysis of the AC components of the collector current can offer an excellent insight into the state space dynamics of our system. For this purpose, we have recorded the time series of the collector current with a sampling rate of 500 kHz delivering 15,000 points in 0.03 s, i.e., the sampling time was $\tau_s = 2\ \mu s$.

Fig. 7 shows the histograms of the signal values, i.e., the number of events in the specified intervals of the collector current. From the strong asymmetry of the histograms #5–#7 we can discern the limitation of the collector current, and we conclude that this is mainly due to the PRI [8].

For analysing the dynamics in the state space of our system, we use the observations of Packard et al. [33], Ruelle [34] and Takens [35], from which we conclude that we do not need the derivatives to form a coordinate system which describes the structure of orbits in phase space. Instead, we can use directly the time advanced variables $s(t + n\tau_s)$, where $n = 1, 2, \ldots, d$, and $\tau = k\tau_s$ is an appropriately chosen time delay, and define the so-called *delay-coordinate vectors*

$$y_n = \{s(t_0 + n\tau_s), s(t_0 + n\tau_s + k\tau_s), \ldots, \times s[t_0 + n\tau_s + k(d-1)\tau_s]\}^T \quad (4)$$

or

$$y_n = \{s_n, s_{n+k}, s_{n+2k}, \ldots, s_{n+(d-1)k}\}^T, \quad (5)$$

where $s_n \equiv s(t_0 + n\tau_s)$, $s_{n+k} \equiv s(t_0 + n\tau_s + k\tau_s)$, etc. T means that the vector is to be transposed.

The space constructed by using the vectors y_n is called the *reconstructed space*. According to a theory of Takens [35] and Mané [36], the geometric structure of the dynamics of the system, from which the s_n were measured, can be observed in the reconstructed d-dimensional Euclidean space if $d \geq 2d_a + 1$, where d_a is the dimension of the attractor of interest. The parameter τ is called *time delay*, the integer d is called the *embedding dimension*, the constructed coordinates are called *delay coordinates*, and this method of constructing coordinates is called the *method of delays*.

There are many systematic approaches for choosing the time delay and the embedding dimension. In our analysis we have used two methods to determine the time delay and one method to determine the embedding dimension. The two methods to determine the time delay, which provide us with the same results, are the autocorrelation function and the average mutual information. The first method says that if the autocorrelation function has a zero crossing at τ, the corresponding value of the time delay is chosen to be τ. Otherwise, the first local minimum of the autocorrelation function is used to specify τ. Fig. 8 shows the autocorrelation functions for our signals labelled #1–#9, taken from the times series #1–#9 of Fig. 3. The results obtained for the time delays are shown in Table 1.

The second method was proposed by Fraser and Swinney [37]. They used concepts of information theory suggested that one should use the time delay corresponding to the first local minimum of the quantity called *mutual information*, which is a function of both linear and non-linear dependencies between two variables. The mutual information is a measure of the information (or predictability) that $s(t)$ can provide about $s(t + \tau)$. The two-dimensional approach of Fraser and Swinney was extended to higher dimensions by Fraser [38]. He introduced a quantity called *redundancy* and suggested choosing a time delay corresponding to minimum redundancy. The results obtained by applying the formalism of Fraser and Swinney are the same as in Table 1.

Table 1
The time delays

	Signal								
	#1	#2	#3	#4	#5	#6	#7	#8	#9
Time delay	$3\tau_s$	$2\tau_s$	$2\tau_s$	$2\tau_s$	$2\tau_s$	$2\tau_s$	$2\tau_s$	$2\tau_s$	$3\tau_s$

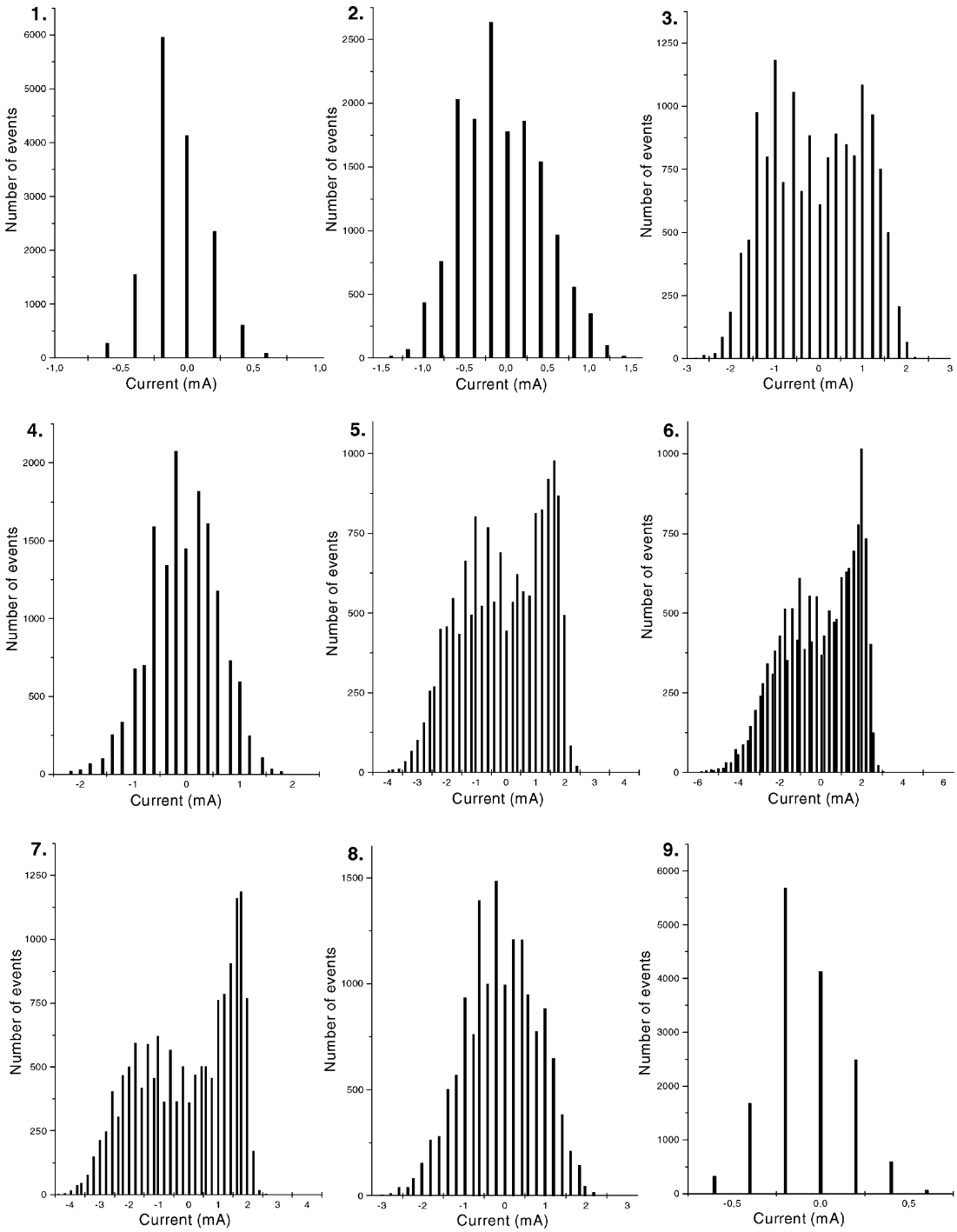

Fig. 7. Histograms of the time series values, showing the number of events vs. the respective values of the collector current.

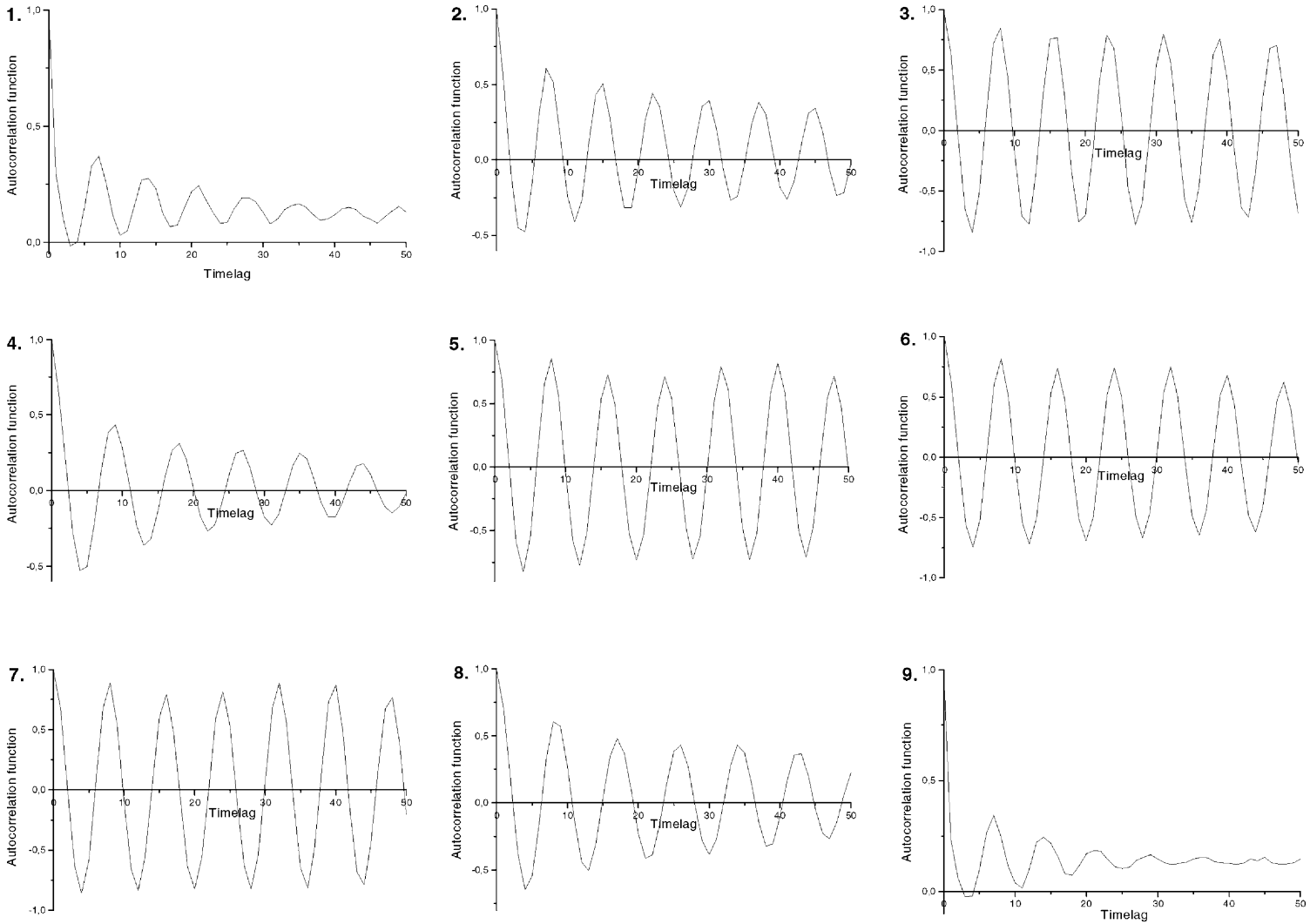

Fig. 8. Autocorrelation function of the time series of Fig. 2.

To determine the embedding dimension we have chosen the method of *false nearest neighbours*, proposed by Kennel et al. [39]. The basic idea underlying the false nearest neighbours approach is to find an embedding space of dimension *d*, in which all false crossings of the orbit with itself that arise because of the projection onto a low-dimension space, are eliminated. When *d* is not large enough, points that are far apart in the original state space are brought close together in the reconstruction space, resulting in false nearest neighbours. To determine these neighbours, one needs to examine if two states are neighbours because of the dynamics or because of the projection onto a low-dimension space. Thus, by determining neighbours in increasing embedding dimension, one can eliminate false neighbours and hence establish the embedding dimension. According to Abarbanel et al. [40], one may choose the embedding dimension to correspond to that value, at which false nearest neighbours drop to below 1%. Using the method described

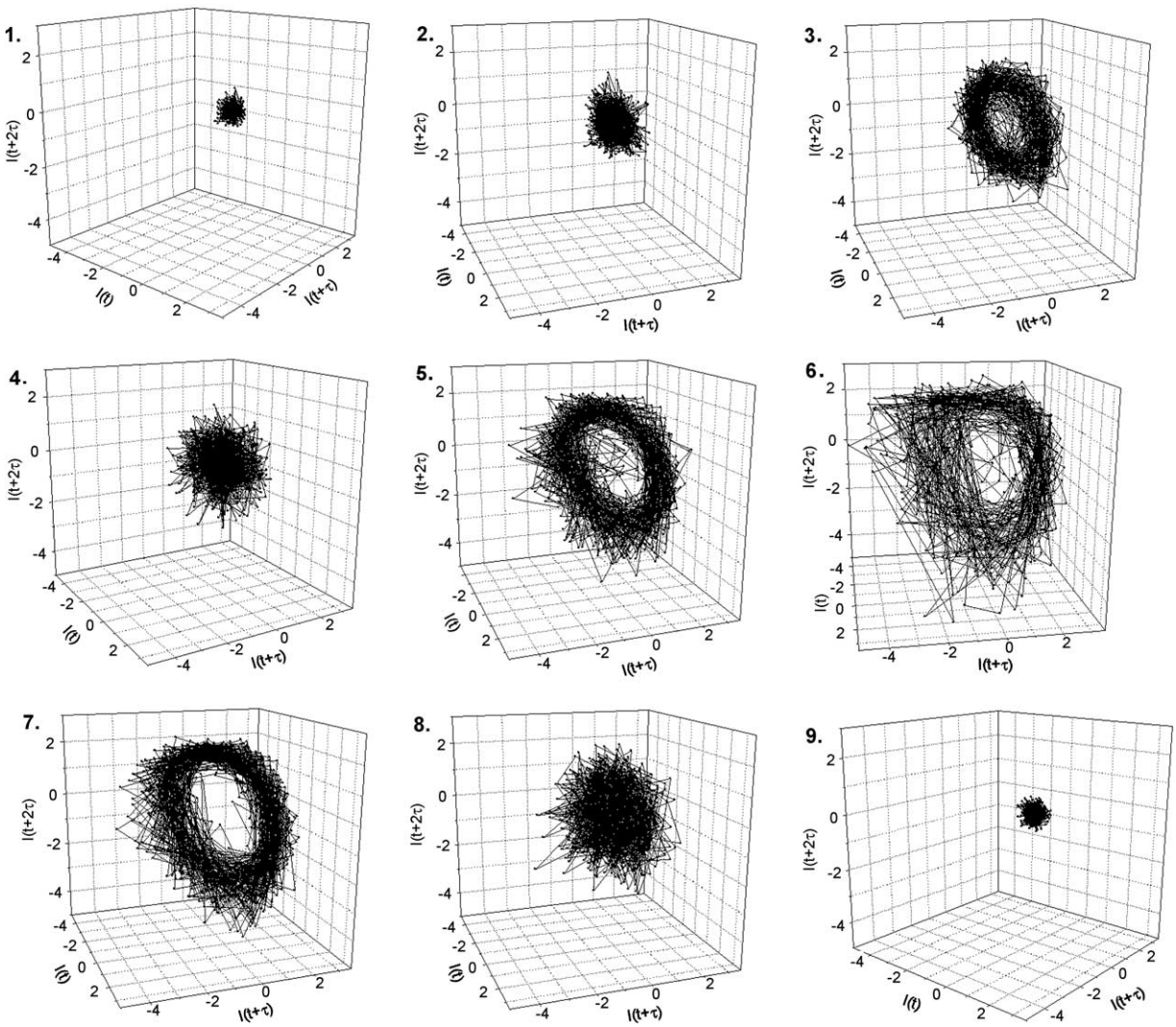

Fig. 9. 3D Poincaré maps of the reconstructed space for the nine cases of Fig. 2.

Table 2
The embedding dimension

	Signal								
	#1	#2	#3	#4	#5	#6	#7	#8	#9
Embedding dimension	1	1	2	1	2	2	2	2	1

above, we have obtained the next values for the embedding dimension, as shown in Table 2.

Now, having the time delay and embedding dimension for each of our signals #1–#9 of Fig. 3, we can plot the reconstructed space, using the method of delays. Fig. 9 shows the 3D Poincaré maps through the reconstructed space. We point out that the trajectories in the phase space, constructed with the derivatives, have almost the same shapes as in Fig. 9.

We emphasise the torus shape of the maps which correspond to the signals #3 and #5–#7. This proves the fact that for these cases indeed we have a system of two coupled non-linear oscillators, where the ratio of the two frequencies corresponds to the ratio of major to minor radius of the respective torus. For the other cases, especially for the cases #1 and #9, where only the EICI is present in the system, the maps contract to almost a point, as it is to be expected.

To describe an amplitude and frequency modulated signal, Nayfeh and Balachandran [41] have proposed an analytical expression given by

$$x(t) = a(t)\,\cos[\omega t + \beta(t)] \tag{6}$$

where

$$a(t) = a_0[1 + \alpha\cos(\omega_m t + \theta)] \quad \text{and}$$
$$\beta(t) = \beta_0\cos(\omega_m t). \tag{7}$$

We used this expression to fit our modulated signal #7, for $\omega = \omega_{\mathrm{EICI}}$ and $\omega_m = \omega_{\mathrm{PRI}}$. As can be seen in Fig. 10, we obtain a very good simulation of the time series #7 for the values: $a_0 = 2.5\,\mathrm{mA}$, $\alpha = 0.4$, $\theta = 0$ and $\beta_0 = 0.7$. So, the function describing this reads

$$x(t) = 2.5(1 + 0.4\cos\omega_{\mathrm{PRI}}t) \times \cos(\omega_{\mathrm{EICI}}t + 0.7\cos\omega_{\mathrm{PRI}}t). \tag{8}$$

Naturally, we obtain a good fit only for the downward part of the signal (the negative excursions of the current), since the upward part of the signal is affected by the effect of current limitation, which cannot be described by the simulation above.

5. Discussion of the frequency behaviour of the EICI

Our experimental results have shown for the first time not only an amplitude modulation like in [26] but also a frequency modulation of the EICI by the PRI and the appearance of sidebands. Moreover, we have found that f_{EICI} depends not only on the magnetic field strength, but also on the collector current, and it turned out that the EICI frequency is approximately negatively proportional to I_{co} (cf. Eq. (3)). The appearance of the EICI and PRI, respectively, seems to be associated with the current jumps together with the hysteresis phenomenon.

To understand the interaction between the two instabilities and the dependence of the EICI frequency on the collector current we refer to an earlier phenomenological model [42], which took into account electron impact reactions in the space charge sheaths related to these phenomena. We recall that both instabilities involve oscillating space charge double layers [8,13–15], which, during one period of the instabilities, are at first created at the positively biased collector, then propagate very fast through the system, and eventually relax on a much slower time scale back towards the collector. During its slow propagation back to the latter, each double layer divides the plasma column into two regions (see also Fig. 1).

- One is located between the collector and the double layer, the relative position of which depends also on the collector bias. In this region the plasma potential is high and the plasma density low.
- The second region is that one between the double layer and the hot plate. There the plasma density is high due to new plasma produced at the hot plate, but the plasma potential is low.

In order to find an explanation for the observed drop of the EICI frequency with increasing collector

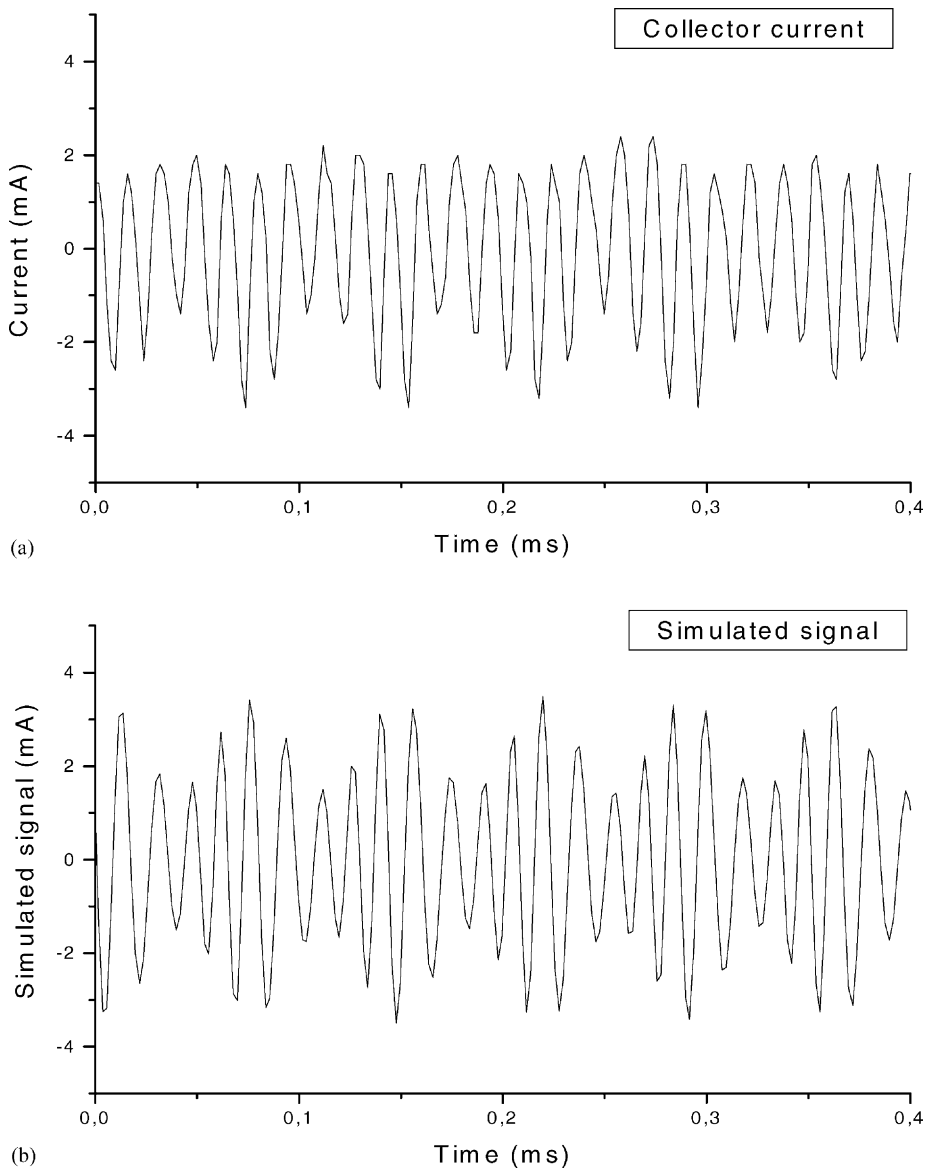

Fig. 10. (a) Time series of the collector current taken at point #7 of the characteristic of Fig. 2; and (b) plot of an amplitude and frequency modulated signal given by $x(t) = 2.5\ (1 + 0.4\cos\omega_{\mathrm{PRI}}t)\ \cos(\omega_{\mathrm{EICI}}t + 0.7\cos\omega_{\mathrm{PRI}}t)$.

current (Fig. 6), we recall that this instability can only be excited with high coherence and amplitude by a collector with a radius smaller than that of the plasma column [13]. In the current channel in front of the collector, the plasma potential jumps upwards during each period of the EICI as soon as a double layer is created there. This is due to the periodical withdrawal of electrons from the plasma in front of the collector during each maximum of the collector current I_{co}, so that a positive space charge remains in the current channel. Thus, during these maxima a radial electric field appears at the edge of the current channel, which

gives rise to the simultaneous radial ejection of ions from the current channel between the double layer and the collector into the surrounding annular plasma. There they form a so-called coherent azimuthal ion ring beam, as it was found by Stern et al. [43] (for a description of the EICI mechanism see also [13]). After this ejection, the ions perform a gyration so that they return into the channel after approximately one gyroperiod. Due to the acceleration of ions during the current maxima by the radial electric field, the time after which the ions re-enter the current channel is somewhat shorter than one gyroperiod. Therefore the trajectories are also not pure circles [44] but rather epitrochoids, and $f_{\mathrm{EICI}} > \Omega_{\mathrm{i}}/2\pi$. Consequently, the strength of this radial field has a strong influence on the EICI frequency, and we find that the frequency is higher for a higher electric field strength. Thus there exists the following logical connection between the positive space charge in the current channel and the EICI frequency.

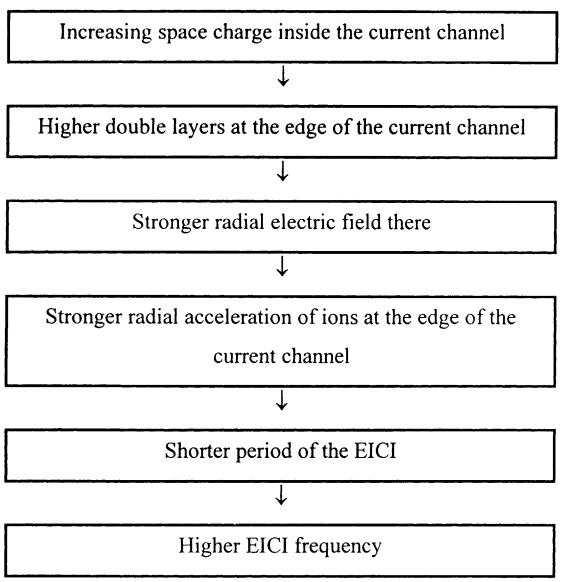

This logical connection works of course also the other way around. If the positive space charge inside the current channel decreases, the EICI frequency will drop. Thus the experimentally observed frequency drop must be an indication that for increasing I_{co} the positive space charge inside the current channel becomes smaller, although this seems to contradict the intuition that for increasing current also the space charge should grow.

However, this apparent contradiction can be explained in the following way: a higher collector current means also a higher and more energetic electron flux towards the collector, and, according to recent findings [23–25], there can be a considerable number of impact reactions (both excitation and ionisation processes) of these electrons with a certain non-negligible background vapour pressure of potassium. Since inelastic collisions like electron excitation and ionisation reactions lead to a loss of kinetic energy of the electrons, on the time average a population of low energetic electrons is dynamically created in the current channel [25]. These in turn cause a reduction of the ion space charge inside the current channel (partly compensating the loss of electrons due to the increased current to the collector) and thus to a drop of the periodical radial electric field, which is involved in the EICI mechanism. Therefore the EICI period increases and the frequency decreases.

Schrittwieser et al. [25] have tried to estimate the partial potassium pressure in the Innsbruck Q-machine by taking into account several effects:

- Under the above-mentioned conditions, the ionisation probability of potassium on tungsten is about 60% [45]. Therefore, and since inevitably a part of the K-beam does not hit the hot plate but slips by, the partial pressure of neutral potassium vapour between the hot plate and the collector can be considerably higher than hitherto presumed.
- The flow conductance of the Q-machine vacuum cylinder under molecular flow conditions is rather low [46]. This, together with the speed of the vacuum pump of 200 L/s leads to the conclusion that there can be a pressure difference of a few times 10^{-4} mbar between the plasma region and the region near the pressure gauge, which is situated about 80 cm from the HP away at the cold end of the Q-machine vacuum cylinder behind a sharp 90° bend of the tube.

- Moreover, most of the potassium atoms, originating from the K-beam, are eventually adsorbed at the water-cooled walls of the cylinder. This could even increase the difference between the partial pressure of K in the plasma region and at the cold end of the Q-machine.

In view of these arguments, the background K-vapour can only be roughly estimated, but in any case the traditional opinion that a Q-machine can be considered collisionless, cannot be maintained.

Following [25], also we estimate the partial potassium vapour pressure in the plasma region to be about 5×10^{-4} mbar and its temperature about 400 K (the K-oven temperature). With these values we obtain a numerical density of $n_K \cong 10^{13}\,cm^{-3}$. With a maximum ionisation cross-section for K of $\sigma_i \cong 8 \times 10^{-16}\,cm^2$ [47], we find a mean free path for electron impact ionisation of $\lambda_{mfp} \cong 125$ cm. Also the cross-sections for electron impact excitation are of a similar order of magnitude. Although λ_{mfp} is about 4.5 times the system length, we have also to take into account that the strong magnetic field extends the effective interaction length. So in spite of the apparently high value of λ_{mfp} it appears that enough electrons are decelerated and can cause a decrease of the positive space charge in the current channel.

In this connection we emphasise that other authors have also observed the strong influence of electron impact reactions at comparably low pressures, e.g., in discharges which worked at pressures as low as 10^{-5} mbar, in spite of the fact that a conventional calculation of λ_{mfp} would also in those cases deliver a value that is higher than the length of the system [48,49]. This is a clear evidence that inelastic collisions can play an essential role even under these conditions.

Our model can also explain the observed frequency modulation of the EICI (Fig. 5) by the PRI and the appearance of sidebands around the EICI frequency. The PRI produces a strong modulation of the collector current (as seen also in Fig. 5), and since the EICI frequency depends on the current, the frequency has to vary with the frequency of the PRI.

6. Conclusion

We presented and analysed new experimental findings showing novel features of two important low-frequency instabilities in a magnetised low-density plasma column: (i) a strong amplitude and frequency modulation of the EICI by the PRI; (ii) the appearance of sidebands around the frequency f_{EICI} with a frequency difference equal to $\pm f_{PRI}$; and (iii) a decrease of the EICI frequency with the collector current.

We also found that in a certain range of the collector current, the two instabilities appear simultaneously and are obviously strongly coupled. This can be understood by the fact that the PRI causes a modulation of the current through the system, while the EICI frequency clearly depends on the collector current. We believe that the double layers, being very complex space charge configurations, which are generated in a Q-machine in front of the positively biased collector, can act as stimulators able to excite different kinds of low frequency instabilities. If the current variations, related to the double layers dynamics, triggered by one of the instabilities, cover the current range of another instability, two independent oscillators are present, in which the oscillations are stimulated by the same source. Under such conditions the oscillators are non-linearly coupled by the common source so that in the spectrum sidebands appear, with frequencies corresponding to the sum and difference of the two instability frequencies.

In addition, we performed a non-linear dynamical analysis of the obtained times series and were able to reconstruct the state space dynamics of our system. We also found a very good analytical fit for one of our time series, thereby obtaining a simulation model of the two coupled oscillators EICI and PRI.

Acknowledgements

This work was supported by the Fonds zur Förderung der wissenschaftlichen Forschung (Austria) under grant No. P-14545-PHY and by the University of Innsbruck. The authors D.-G.D., V.I., E.L. and

M.S. would like to thank the members of the Innsbruck Experimental Plasma Physics Group at the University of Innsbruck for their cordial hospitality during their stays. The work of two of the authors (D.-G.D. and V.I.) was carried out in the framework of ERASMUS-SOCRATES and CEEPUS programmes.

References

[1] N. Rynn, N. D'Angelo, Rev. Sci. Instrum. 31 (1960) 1326.
[2] R.C. Knechtli, J.Y. Wada, Phys. Rev. Lett. 6 (1961) 215.
[3] N.S. Buchelnikova, R.V. Salimov, Sov. Phys. JETP 29 (1969) 595.
[4] J.P. Hauck, N. Rynn, G. Benford, Phys. Fluids 16 (1973) 1946.
[5] N. Sato, H. Ikezi, N. Takahashi, Y. Yamashita, Phys. Rev. 183 (1969) 278.
[6] F. Cap, Handbook on Plasma Instabilities, vols. I–III, Academic Press, 1976.
[7] S. Kuhn, Contrib. Plasma Phys. 34 (1994) 495.
[8] S. Iizuka, P. Michelsen, J.J. Rasmussen, R. Schrittwieser, R. Hatakeyama, K. Saeki, N. Sato, Phys. Rev. Lett. 48 (1982) 145.
[9] G. Chanteur, M. Raadu, Phys. Fluids 30 (1987) 2708.
[10] D.M. Suszynsky, S.L. Cartier, R.L. Merlino, N. D'Angelo, J. Geophys. Res. 91 (1986) 729.
[11] F.F. Chen, Plasma Phys. 7 (1965) 399;
H.W. Hendel, T.K. Chu, P.A. Politzer, Phys. Fluids 11 (1968) 2426;
P.A. Politzer, Phys. Fluids 14 (1971) 2410.
[12] G.I. Kent, N.C. Jen, F.F. Chen, Phys. Fluids 12 (1969) 2140; F.W. Perkins, D.L. Jassby, Phys. Fluids 14 (1971) 102.
[13] J.J. Rasmussen, R. Schrittwieser, IEEE Trans. Plasma Sci. 19 (1991) 457.
[14] G. Popa, R. Schrittwieser, J.J. Rasmussen, P. Krumm, Plasma Phys. Contrib. Fus. 27 (1985) 1063.
[15] N. Sato, R. Hatakeyama, J. Phys. Soc. Japan 54 (1985) 1661; R. Hatakeyama, F. Muto, N. Sato, Jpn. J. Appl. Phys. 24 (1985) L285.
[16] M.E. Koepke, W.E. Amatucci, J.J. Carol III, T.E. Sheridan, Phys. Rev. Lett. 72 (1994) 3355.
[17] N. Rynn, Phys. Fluids 5 (1962) 634;
N. Rynn, Phys. Fluids 9 (1966) 165.
[18] N. Sato, G. Popa, E. Märk, E. Mravlag, R. Schrittwieser, Phys. Fluids 19 (1976) 70;
R. Schrittwieser, Phys. Lett. 65A (1978) 235.
[19] R. Schrittwieser, Int. J. Mass Spectrom. Ion Process. 129 (1993) 205.
[20] S. Iizuka, P. Michelsen, J.J. Rasmussen, R. Schrittwieser, R. Hatakeyama, K. Saeki, N. Sato, J. Phys. Soc. Japan 54 (1985) 2516.
[21] P. Michelsen, H. Pécseli, J.J. Rasmussen, R. Schrittwieser, Plasma Phys. 21 (1979) 61.
[22] M.E. Koepke, M.J. Alport, T.E. Sheridan, W.E. Amatucci, J.J. Carroll III, Geophys. Res. Lett. 21 (1994) 1011.
[23] C. Avram, R. Schrittwieser, M. Sanduloviciu, Int. J. Mass Spectrom. 184 (1999) 129;
C. Avram, R. Schrittwieser, M. Sanduloviciu, Contrib. Plasma Phys. 39 (1999) 223.
[24] C. Avram, R. Schrittwieser, M. Sanduloviciu, J. Phys. D: Appl. Phys. 32 (1999), 2750 and 2758.
[25] R. Schrittwieser, C. Avram, P.C. Balan, V. Pohoaţà, C. Stan, M. Sanduloviciu, Physica Scripta T84 (2000) 122.
[26] R. Schrittwieser, Phys. Fluids 26 (1983) 2250.
[27] C. Winkler, D. Strele, S. Tscholl, R. Schrittwieser, Plasma Phys. Contrib. Fus. 42 (2000) 217.
[28] W.E. Drummond, M.N. Rosenbluth, Phys. Fluids 5 (1962) 1507.
[29] S. Iizuka, R. Schrittwieser, Phys. Lett. 149A (1990) 393;
S. Iizuka, R. Schrittwieser, Plasma Phys. Contrib. Fus. 35 (1993) 77.
[30] T. Gyergyek, M. Čerček, M. Stanojević, N. Jelić, Contrib. Plasma Phys. 33 (1993) 53;
T. Gyergyek, M. Čerček, M. Stanojevié, N. Jelić, J. Phys. D Appl. Phys. 27 (1994) 2080.
[31] G. Popa, R. Schrittwieser, Plasma Phys. Contrib. Fus. 38 (1996) 2155.
[32] D.R. Dakin, T. Tajima, G. Benford, N. Rynn, J. Plasma Phys. 15 (1976) 175.
[33] N.H. Packard, J.P. Crutchfield, J.D. Farmer, R.S. Shaw, Phys. Rev. Lett. 45 (1980) 712.
[34] D. Ruelle, Chaotic Evolution and Strange Attractors, Cambridge University Press, 1989.
[35] F. Takens, in: D.A. Rand, L.S. Young (Eds.), Dynamical Systems and Turbulence, Lecture Notes in Mathematics, Vol. 898, Springer-Verlag, 1981.
[36] R. Mané, in: D.A. Rand, L. S. Young (Eds.), Dynamical Systems and Turbulence, Lecture Notes in Mathematics, Vol. 898, Springer-Verlag, 1981.
[37] A.M. Fraser, H.L. Swinney, Phys. Rev. A 33 (1986) 1134.
[38] A.M. Fraser, IEEE Trans. Inf. Theory 35 (1989) 245;
A.M. Fraser, Physica D 34 (1989) 391.
[39] M.B. Kennel, R. Brown, H.D.I. Abarbanel, Phys. Rev. A 45 (1992) 3403.
[40] H.D.I. Abarbanel, R. Brown, J.J. Sidorowich, L.S. Tsimring, Rev. Mod. Phys. 65 (1993) 1331.
[41] A.H. Nayfeh, B. Balachandran, Applied Nonlinear Dynamics–Analytical, Computational and Experimental Methods, Wiley, New York, 1995.
[42] M. Sanduloviciu, R. Schrittwieser, C. Ioniţă, E. Lozneanu, D. Dimitriu, V. Ignatescu, J. Plasma Fus. Res. SERIES 4, 2001, in press.
[43] R.A. Stern, D.N. Hill, N. Rynn, Phys. Rev. Lett. 47 (1981) 792.
[44] J.J. Rasmussen, R.W. Schrittwieser, T. Kobayashi, Proceedings of Workshop on the Current-Driven Electrostatic Ion–Cyclotron Instability, Innsbruck, 1987, World Scientific (1988) 152.

[45] R. Schrittwieser, R. Koslover, R. Karim, N. Rynn, J. Appl. Phys. 58 (1985) 598.
[46] S. Dushman, Scientific Foundations of Vacuum Technique, 2nd edition, Wiley, New York, London, Sydney, 1949.
[47] H. Deutsch, K. Becker, T.D. Märk, Int. J. Mass Spectrom. 185–187 (1999) 319.
[48] S. Cartier, R.L. Merlino, Phys. Fluids 30 (1987) 2549.
[49] H. Gunnell, R. Schrittwieser, S. Torvén, Phys. Lett. A 241 (1998) 281.